



Selenoxide elimination manipulate the oxidative stress to improve the antitumor efficacy



Chenxing Sun^a, Lu Wang^a, Banruo Xianyu^a, Tianyu Li^a, Shiqian Gao^{a,b,**}, Huaping Xu^{a,*}

^a Key Laboratory of Organic Optoelectronics and Molecular Engineering, Department of Chemistry, Tsinghua University, Beijing, 100084, China

^b Tsinghua-Peking Joint Center for Life Sciences, Beijing, 100084, China

ARTICLE INFO

Keywords:

ROS
β-Selene diesters
Selenoxide elimination
Oxidation therapy

ABSTRACT

Selenoxide elimination reaction has been widely used in the field of organic synthesis. However, few studies have been conducted to apply this reaction in biodegradable nanomedicine. In this work, the selenoxide elimination reaction was used for cancer treatment via producing excess cellular reactive oxygen species (ROS) for the first time. The β-selene diesters and porphyrin derivatives containing nanoparticle could be responsive to the intracellular ROS and produce acrylates through the elimination reaction. The acrylates would further deplete intracellular GSH in tumor cells and finally improved the anticancer activity in the mice tumor model. Different from traditional ROS-responsive nanomedicine, the elimination product of this reaction could regenerate cytotoxic ROS and specifically disturb the redox balance of tumor cells. This work would provide attractive avenues for the development of therapeutic strategies against cancer via synthesis of well-designed biodegradable polymers.

1. Introduction

Reactive oxygen species (ROS) act as a second messenger in cell signalling and are essential in supporting various cellular processes, such as differentiation, proliferation, metabolism and apoptosis [1,2]. Excess ROS production induced by endogenous or exogenous stimuli, leads to aberrant cell signalling and the disruption of cellular homeostasis. Owing to oncogenic transformation, cancer cells can constantly generate higher levels of intracellular ROS (up to 100 μM) than normal cells (approximately 20 nM) [3,4]. Cancer cells can maintain intracellular redox homeostasis through their inherently flexible redox regulation [5]. However, compared to normal cells, the high levels of exogenous ROS in cancer cells makes them more vulnerable to reach a threshold that triggers death [6]. Therefore, ROS-based cancer therapy approaches aimed at generating ROS targeted in tumor cells may further improve selective therapeutic efficiency in cancer cells.

The mechanism that underlies the ROS-based therapy exerted on killing cancer cells is associated with elevated ROS levels that leads to irreversible oxidative stress in tumor cells. Recently, many strategies have been developed to increase the intracellular ROS levels in cancer cells [7]. Photosensitizers or atomically dispersed metals have already been employed to generate toxic levels of ROS in tumor cells,

respectively, in photodynamic therapy (PDT) [8–10] and chemodynamic therapy (CDT) [11–13]. ROS-responsive components, including selenide/telluride [14,15], disulphide/selenide [16–19], thioketal [20], thioether [21], and arylboronic ester [22] etc, containing polymers are widely used in these therapies to improve the targeting responsiveness of nanodrugs in tumor cells [23–25]. Ironically, the elevated ROS levels will quickly be neutralized by the intracellular antioxidant defense system, such as glutathione (GSH), and could also be consumed by these ROS-responsive linkers [26,27]. These endogenous and exogenous ROS consumptions would interfere with the therapeutic effect of ROS-based therapy and enhance the drug resistance of chemotherapy. Therefore, it is urgent to find a novel ROS-response chemical reaction or linker to weaken the antioxidant defense systems and elevate intracellular ROS generation after the response, leading to massive ROS accumulation, to improve the efficacy of ROS-manipulation mediated cancer therapy.

Acrylates, such as 2-hydroxyethyl methacrylate (HEMA) and triethylglycol dimethacrylate (TEGDMA) was reported to chemically react with antioxidant GSH, depleting intracellular GSH, increasing ROS levels and leading to cell apoptosis [28,29]. In our previous work [30], we found that β-selene diesters could be oxidized to acrylate by ROS, such as hydrogen peroxide (H₂O₂), which was similar to the

* Corresponding author.

** Corresponding author. Key Laboratory of Organic Optoelectronics and Molecular Engineering, Department of Chemistry, Tsinghua University, Beijing, 100084, China.

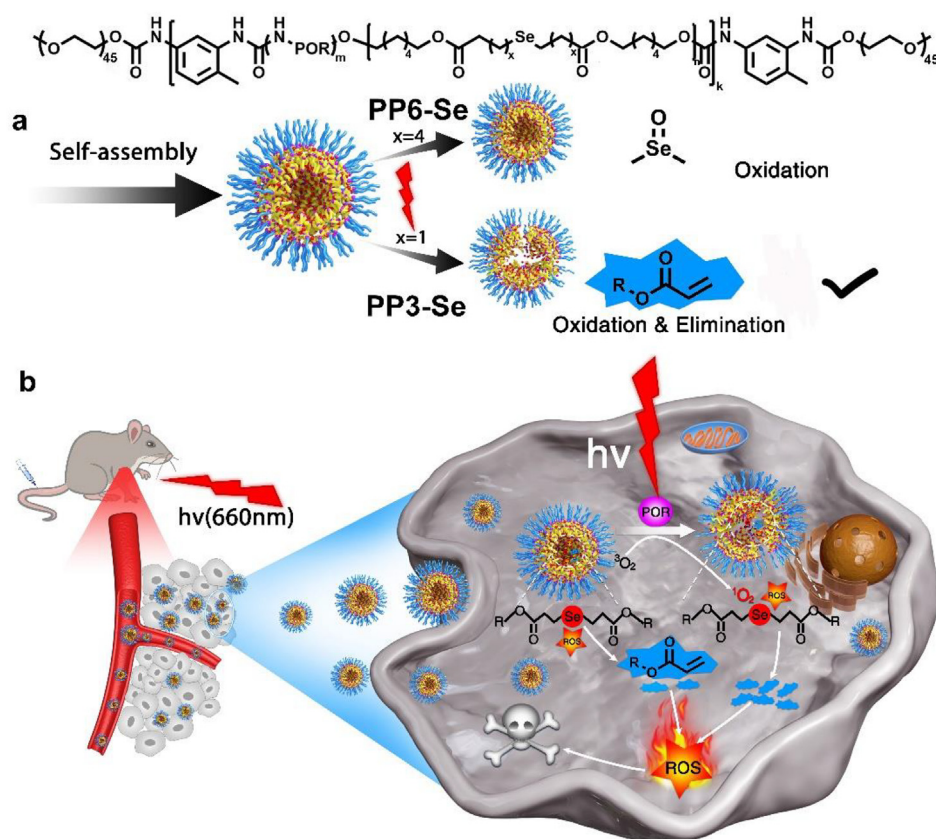
E-mail address: xuhuaping@tsinghua.edu.cn (H. Xu).

<https://doi.org/10.1016/j.biomaterials.2019.119514>

Received 1 July 2019; Received in revised form 9 September 2019; Accepted 20 September 2019

Available online 24 September 2019

0142-9612/ © 2019 Published by Elsevier Ltd.



Scheme 1. Schematic illustration of selenoxide elimination induced ROS-manipulation for antitumor therapy. a) The selenium-containing polymers can self-assemble into nanoparticles in aqueous solution. Only β -seleno diesters ($x = 1$), can be eliminated after oxidation by $^1\text{O}_2$, to generate acrylate. While the δ -substituted one could only be oxidized to selenoxide. b) MDA-MB-231 cell-bearing nude mice were intravenously injected with the PP3-Se nanoparticles. Due to the EPR effect, PP3-Se nanoparticles could be accumulated in tumor cells. β -seleno diesters in polymeric nanoparticles could be oxidized by intracellular ROS to generate acrylate. When light was introduced, the selenoxide elimination reaction could be accelerated to produce more acrylate. Acrylate could regenerate the ROS level in tumor cells and further reduce the tumor volume.

selenoxide elimination discovered by Sharpless in 1973 [31]. Hence, in this work, the selenoxide elimination reaction was introduced into cancer therapy for the first time. β -Seleno diesters were copolymerized with porphyrin (Por) and terminated by polyethylene glycol (PEG) to prepare amphiphilic polymers (PP3-Se). Polymer (PP6-Se) with the replacement of β -seleno diesters by δ -substituted one was also prepared as control. Both of them could self-assemble into nanoparticles in an aqueous solution. A photosensitizer, Por, was employed for intracellular imaging and generating exogenous ROS, especially singlet oxygen ($^1\text{O}_2$) [32]. Under the irradiation of near-infrared (NIR) light, the PP3-Se and PP6-Se polymeric nanoparticles could be oxidized by ROS from the tumor microenvironment and light-induced $^1\text{O}_2$. PP3-Se could be further eliminated to acrylate, which act as an antioxidant inhibitor, consuming intracellular GSH and replenishing the ROS levels in tumor cells to induce cancer cell apoptosis (Scheme 1). The combination of this ROS-triggered cytotoxicity from the molecular structure itself and photoinduced ROS generation provides a new opportunity for improving antitumor efficiency in ROS-manipulation-mediated cancer therapies.

2. Experiments part

2.1. General information

1,6-Hexanediol, 3-Bromopropionyl Chloride and 6-Bromohexanoylchloride were purchased from J&K Scientific, Tokyo Chemical Industry (Shanghai) and Alfa Aesar, respectively. Selenium powder (Aladdin), NaBH_4 (Aladdin) and Toluene-2,4-diisocyanate (TDI, 98%) were used as received. Poly(ethylene glycol) monomethyl ether (PEG) (Aladdin, average $M_w = 2000$) was dried under 100 °C vacuum before use. Meso-Tetraphenylporphyrin (TPP) was purchased from 9 Ding Chemistry. Trifluoroacetic acid, Tetrahydrofuran (THF), N,N-Dimethylformamide (DMF) and other solvents were purchased from J&K Scientific. Cell Counting Kit-8 (CCK-8) was purchased from

Dojindo Laboratories. Cell Cycle and Apoptosis Analysis Kit and Caspase 3,8 Activity Assay Kit were brought from Beyotime. LysoTracker Green DND-26, Annexin V-FITC/PI Apoptosis Detection Kit, and Reactive Oxygen Species Assay Kit were purchased from YEASEN. Singlet Oxygen Sensor Green Reagent was obtained from life technologies. Primary antibody Bax and Bcl2 were brought from Santa Cruz. Secondary antibody HRP-conjugated rabbit anti-mouse IgG was purchased from CST. TUNEL kit was obtained from Roche. 4',6-diamidino-2-phenylindole (DAPI) was purchased from Beijing Solarbio Science & Technology Co., Ltd. (item no. C0060).

^1H NMR or ^{13}C NMR spectra were obtained in dimethylsulfoxide- d_6 or deuteriochloroform solution, using BRUKER ASCEND™ 400 spectrometer. The GPC results were analysed using a Waters 2414 Index Detector. The hydrodynamic size values of nanoparticles were measured using a Malvern Zetasizer Nano ZS90. Transmission electron microscopy (TEM) was analysed using a JEPL JEM-2010 microscope. A PHI Quantera scanning X-ray microprobe were employed to analyse the valence state of Selenium. Fluorescence spectra were obtained by using an RF-5301PC spectrophotometer (Shimadzu, Japan). Flow cytometry were performed using the BD FACSAria III. And the inductively coupled plasma mass spectrometry (ICP-MS) was detected by ELAN DRC-e ICP Mass Spectrometer.

2.2. Synthesis of 5, 10(15)-bis (4-aminophenyl)-15,20-diphenylporphyrin

To a solution of TPP (0.5 g, 0.815 mmol) in TFA (30 mL) was added sodium nitrite (NaNO_2) (0.458 g, 8.1 equiv.). After 2 min stirring at room temperature, the reaction was terminated by water (40 mL) and further extracted with dichloromethane (DCM) until the colour of water almost disappeared. The organic layers were washed with saturated aqueous NaHCO_3 and then dried over anhydrous Na_2SO_4 . This residue was purified on a plug of silica gel, eluting with DCM: petroleum ether (PE) from 1:1 to 2:1 to pure DCM. After evaporation of solvent under vacuum, the purple powder was dissolved into concentrated

hydrochloric acid (HCl) (30 mL). Tin (II) chloride (1.428 g) was added, while stirring, and the mixture was then heated to 65 °C for 4 h after reaction, the mixture was poured into ice water (100 mL) and further neutralized with ammonium hydroxide until pH = 8. The mixed solution was then extracted with DCM until colorless. The organic layer was concentrated under vacuum and further purified by column chromatography isolation using DCM: ethyl acetate (EA) = 4:1 as elution to give 100 mg purple mixture of 5, 10(15)-bis (4-aminophenyl)-15,20-diphenylporphyrin.

¹H NMR (400 MHz, DMSO-*d*₆) δ (ppm) 8.95 (d, *J* = 6.1 Hz, 4H), 8.78 (d, *J* = 7.2 Hz, 4H), 8.22 (dt, *J* = 7.6, 2.4 Hz, 4H), 7.86 (dtd, *J* = 10.0, 5.4, 4.7, 2.2 Hz, 10H), 7.01 (dd, *J* = 8.4, 3.0 Hz, 4H), 5.60 (d, *J* = 4.2 Hz, 4H), -2.80 (d, *J* = 4.3 Hz, 2H). ¹³C NMR (400 MHz, DMSO-*d*₆) δ (ppm): 149.12, 141.99, 141.91, 136.03, 135.98, 134.67, 131.82, 128.97, 128.86, 128.41, 127.43, 122.16, 121.66, 119.93, 119.48, 113.04, 113.02, 101.59. HR-MS (ESI+), calcd. 644.26885, Found: 645.27667 (M + H⁺).

2.3. Synthesis of bis(6-hydroxyhexyl) 3,3'-selenodipropionate and bis(6-hydroxyhexyl) 6,6'-selenodihexanoate

3-Bromopropionyl Chloride (3.428 g, 20 mmol) was added dropwise with stirring to a solution of 1,6-hexanol (2.3636 g, 20 mmol) in anhydrous tetrahydrofuran (THF) (20 mL) in ice water bath. The resulting solution was stirred at room temperature for 12 h. After evaporation of THF, the colourless oil was purified on a plug of silica gel, eluted with EA:PE (from 1:3 to 1:2). After evaporation of the solvent, the residue was dissolved into THF (20 mL) and then added into an aqueous solution of selenium (0.5 equiv.) and sodium borohydride (4 equiv.). The mixture solution was stirred at 50 °C overnight, and then extracted by DCM (3*50 mL). After evaporation of solvent, the faint yellow oil was purified through column chromatography isolation, eluting with EA:PE (from 1:1 to 2:1).

¹H NMR (400 MHz, Chloroform-*d*) δ 4.09 (t, *J* = 6.6 Hz, 4H), 3.62 (t, *J* = 6.6 Hz, 4H), 2.81 (dd, *J* = 7.7, 5.8 Hz, 4H), 2.71 (dd, *J* = 7.7, 5.8 Hz, 4H), 1.61–1.51 (m, 8H), 1.39 (p, *J* = 3.5 Hz, 8H). ¹³C NMR (400 MHz, CDCl₃) δ (ppm): 172.30, 64.79, 62.70, 35.82, 32.51, 28.63, 25.80, 25.44, 18.01. HR-MS(ESI+), calcd. 426.15206, Found: 449.14122 (M + Na⁺).

Bis(6-hydroxyhexyl) 6,6'-selenodihexanoate was prepared and purified in the similar way.

¹H NMR (400 MHz, Chloroform-*d*) δ 4.07 (t, *J* = 6.7 Hz, 4H), 3.64 (t, *J* = 6.6 Hz, 4H), 2.55 (t, *J* = 7.4 Hz, 4H), 2.31 (t, *J* = 7.4 Hz, 4H), 1.74–1.56 (m, 12H), 1.53–1.32 (m, 16H). ¹³C NMR (400 MHz, CDCl₃) δ (ppm): 173.80, 64.40, 62.80, 34.32, 32.70, 30.40, 29.55, 28.80, 25.88, 25.49, 24.66, 23.81. HR-MS(ESI+), calcd. 510.24596, Found: 533.23519 (M + Na⁺).

2.4. Synthesis of PP3-Se, PP6-Se, and poly-C6-C3(6)-Se-PEG2k

100 mg 5, 10(15)-bis (4-aminophenyl)-15,20-diphenylporphyrin and 330.1 mg bis(6-hydroxyhexyl) 3,3'-selenodipropionate was dissolved in 5 mL of anhydrous DMF in a 100 mL flask and sealed with a rubber plug. A solution of TDI (200 μL) in 10 mL anhydrous DMF was injected to the flask under the atmosphere of nitrogen. After stirring for 6 h at 50 °C, 376 mg PEG dissolved in 10 mL anhydrous DMF was added into this flask and the reaction was carried out for another 24 h. The resulting products were washed by water and ethyl alcohol for three times, respectively, followed by drying under vacuum to give a purple sticky-solid.

PP6-Se, and Poly-C6-C3(6)-Se-PEG2k were prepared and purified in the similar way.

2.5. Preparation of polymeric nanoparticles

20 mg of Se-polymers were first dissolved into 4 mL dimethyl

sulfoxide, and then added into 10 mL of deionized water dropwise under ultrasonication. Subsequently, the polymeric nanoparticles were purified through 48 h dialysis (molecular cut off = 3.5 k), and finally diluted to pre-determined concentration.

2.6. Singlet oxygen generation

Singlet oxygen sensor green (SOSG) was employed to detect the generation of ¹O₂, which could be oxidized by ¹O₂, followed by enhancement of fluorescence, with excitation peaks at 504 nm and emission peaks at 525 nm. Solution of PP3-Se with SOSG (~10 μM) was irradiated with a 660 nm laser at a power density 1.0 W/cm² for 2 or 4 min. The fluorescence intensity was recorded by RF-5301PC SPECTROFLUOROPHOTOMETER (SHIMADZU).

¹O₂ levels were detected by the EPR trapping technique using 2,2,6,6-tetramethyl-4-piperidone (TEMP) as a spin trap. After irradiated with a 660 nm laser at a power density 1.0 W/cm² for 2 or 10 min, the EPR spectra was recorded by JES-FA200 ESR Spectrometer.

2.7. Cell culture

Cell lines MDA-MB-231 (human breast cancer cells), A549 (human lung cancer cells) and L-02 (human hepatocyte cells) were cultured in DMEM supplied with 10% (v/v) FBS, streptomycin (100 μg/mL) and penicillin (100 U/mL). Cells were incubated at 37 °C in a humidified 5% CO₂ atmosphere.

2.7.1. In vitro cytotoxicity and apoptosis

CCK-kit 8: MDA-MB-231, A549 and L-02 cells were seeded on 96-well plates (7000 cells per well). After seeding for overnight, the cells were cultured with various drug formulations for pre-determined time (e.g. 48 h or 72 h). The cell viability was evaluated by CCK-8 kit assay according to the manufacturer's instructions.

Apoptosis: MDA-MB-231 cells were seeded on 6-well plates (for HHA) or 24-well plates (for polymeric nanoparticles) at a density of 200 k or 80 k cells per well. After seeding 12 h, the cells were then co-incubation with various drug formulations for 24 or 48 h (for HHA) or for 4 h for PP3-Se or PP6-Se nanoparticles. To polymeric nanoparticles group, we then irradiated the well for a certain time (660 nm laser, 0.75 W/cm²), and further cultured for 48 h. Cells were then stained with Annexin V-FITC/PI Apoptosis Detection Kit, and further analysed by FCM.

2.8. Cell uptake and intracellular distribution

Cell uptake: MDA-MB-231 cells were seeded at a density of 100 k per well onto 12-well plates, and then co-incubation with PP3-Se nanoparticles (100 μg/mL) for 4, 8 or 24 h. The medium was then washed by phosphate buffer saline (PBS) for three times and then replaced with fresh medium. The cells were incubated with 1 mL trypsin for 1 min, and then centrifugated to collect cells and then resuspended into 2 mL PBS. Owing to the fluorescence imaging ability of Por, FCM was employed to analyse the cell uptake ability.

Intracellular distribution: MDA-MB-231 cells were seeded at a density of 100 k cells per well onto a glass-bottom dish with 2 mL medium and then cultured overnight. The cells was then incubated with PP3-Se nanoparticles (100 μg/mL) for 4 or 24 h at the dose of 19 μg/mL Por at 37 °C. And then the cells were washed by PBS for three times, and replaced with 1.0 mL fresh medium, which was contained with Hoechst 33343 (1.0 μg/mL) and LysTracker Green DND-26 (100 nM). After 20 min incubation, the cells were washed by PBS for three times before CLSM observation (Leica SP8).

2.9. ROS detection

MDA-MB-231 cells were seeded at a density of 80 k cells per well

into 24-well plates and incubated overnight in 2 mL medium. The medium was replaced with fresh medium, followed by addition of PP3–Se nanoparticles (100 µg/mL). The cells were then co-incubated for 4 h, before irradiated with red laser (660 nm laser, 0.75 W/cm²) for total 4 min with 1 min interval after 1 min laser exposure. ROS probe (DCFH-DA) was added into the medium with a final concentration (10 µM) immediately or 20 h after irradiation. To evaluate ROS generation, cells were washed with ice-cold PBS for three times, and then detached by trypsin, harvested and resuspended in PBS for FCM. For FCM, Por was excited with 488 nm laser and emission at 660 nm. The emission wavelength of DCFH-DA was set at 530 nm (excited with 488 nm). Data were analysed with Flowjo Software.

2.10. Western blot

MDA-MB-231 cells were seeded at a density of 10 k cells per well onto 24-well plates, and then cultured overnight before treated with PP3–Se or PP6–Se nanoparticles. The cells were then co-incubated with nanoparticles for 4 h and subsequently irradiated with red laser (660 nm laser, 0.75 W/cm²) for total 4 min with 1 min interval after 1 min laser exposure. And further cultured for 10 min, 12 h or 20 h, the total intracellular protein was extracted with RIPA buffer and loaded into 12% polyacrylamide SDS-PAGE gel. Protein was further transferred to nitrocellulose membrane in SDS-electroblot buffer. The membrane was then washed by TBS for three times and blocked by 5% BSA solution for 1 h at room temperature. And then the membrane was immunoblotted with primary antibodies (*anti-Bax* or *Bcl2* and *anti-Tubblin*) overnight at cold temperatures. After five times washed with TBST (TBS with 0.1% tween), the membrane was incubated with secondary antibodies at room temperature for another 1 h. The membrane was washed by TBST for three times (5 min per time), and then visualized by enhanced chemiluminescence (ECL).

To HHA group, the cells were incubated with 300 µM HHA for 10 min, 12 h or 24 h. And we then analysed the regulation of Bax or Bcl2 proteins in cells by Western blot analysis followed above methods.

2.11. Caspase activity detection

The activation of caspase 3 or 8 in MDA-MB-231 cells were determined by using corresponding kits under the manufacturer's instructions. BCA kit was also employed to evaluate the protein concentration in each group.

2.11.1. Exo vivo fluorescence imaging

The BALB/c nu/nu mice (4 weeks old) with tumor xenograft was first injected with PP3–Se nanoparticles (11.1 mg/kg) via lateral tail vein and then scarified after 4 or 24 h post-injection. The tumor, kidney, liver, lung, spleen and heart were removed for *ex vivo* fluorescence imaging using a IVIS lumina II *in vivo* spectrum imaging system at an excitation 488 nm. And meanwhile we also employed ICP-MS to determine the selenium concentrations.

2.11.2. In vivo anti-tumor effect

Breast cancer tumor xenografts were formed in to the BALB/c nu/nu mice (4 weeks old) orthotopically by injecting MDA-MB-231 cells with a density of 2000 k into the breast (7 mice/group). When the tumor volume reached about 100 mm³, the mice were injected with various drug formulations, including saline, PP3–Se nanoparticles and PP6–Se nanoparticles, on every three days. The laser treatment was carried out for a total 4 or 10 min at a power density of 0.75 W/cm² with 1 min interval after every 2 min laser exposure 24 h after pro-administration. Tumor size was measured using Vernier calipers, and tumor volume were calculated using formula $V = 1/2 ab^2$, where a represents the long axis and b is short axis. The body weight was measured simultaneously to evaluated the side effects of polymers. After 46 days, the mice were scarified and the tumor xenografts were excised for following

experiments.

2.12. Side effects on mice

To study the side effects of PP3–Se nanoparticles with or without light irradiation *in vivo* in our work, at 46 days, another three mice in each group were anesthetized and various organs and serum were collected for further study. H&E staining were employed to study the potential organ morphology changes in kidney, liver, lung, spleen and heart. Serum was used for blood chemistry and haematology analysis.

2.13. Statistical analysis

GraphPad Prism 7 was used for statistical analyses. The statistical differences between mean values were determined by one-way analysis of variance (ANOVA). A probability level of 95% (P value < 0.05) was considered statistically.

2.14. Safety statement

No unexpected or unusually high safety hazards were encountered.

3. Results and discussion

Synthesis and preparation of PP3–Se nanoparticles. The synthesis of monomers and polymers is described in detail in the Experimental Section in Supporting Information [SI]. Briefly, we first synthesized the ROS-responsive eliminable amphiphilic ABA triblock copolymer (PP3–Se), which consisted of both hydrophobic segments containing bis(6-hydroxyhexyl) 3,3'-selenodipropionate and porphyrin (ester: por = 5:1) and hydrophilic PEG ($M_w = 2$ kg/mol) segment (Fig. S1). For comparison, a control polymer (PP6–Se) was also prepared to further show the unique properties of the selenoxide elimination reaction. Another two ABA type block copolymers, Poly-C6-C3-Se and Poly-C6-C6-Se, were also synthesized for porphyrin-free nanoparticles to study the influence of porphyrin. ¹H NMR (Fig. S2a, Fig. S4a and Fig. S5b) and gel permeation chromatography (GPC) (Fig. S2b, Fig. S4b and Fig. S5a) confirmed the successful synthesis of the polymers, indicating that PP3–Se and PP6–Se had molecular weights (M_w) of 34 k and 37 k, respectively. The total concentration of Por in PP3(6)-Se was determined to be 0.192(0.11) mg/mg, according to the method described in our previous work [33].

The nanoparticles were prepared through a dialysis method. Dynamic light-scattering (DLS) measurements showed that both PP3–Se and PP6–Se could self-assemble in aqueous solution with hydrodynamic diameters of approximately 69 nm and 125 nm (Fig. 1a, Fig. S4c), respectively. Transmission electron microscopy (TEM) images showed that these nanoparticles were spherical micelles (Fig. 1b, Fig. S4d). Both of PP3–Se and PP6–Se could be well-dispersed in aqueous solutions, such as phosphate-buffered saline (PBS) or DMEM, and their mean count rate remained almost unchanged even after incubation for one week, indicating the stability in physiological environment (Fig. S7a). As indicated by the DLS results, the critical aggregation concentration (CAC) of PP3–Se was 1.53×10^{-3} g/L (Fig. S2c). The UV/Vis absorption spectrum of PP3–Se nanoparticles in dimethyl formamide (DMF) displayed an absorption peak in the red region (600–700 nm) (Fig. 1c). For high tissue penetrability and minimal phototoxicity, a 660 nm laser was chosen to be used in the following experiments. Additionally, the PP3–Se nanoparticles maintained the bioimaging capability of porphyrin derivatives (excitation/emission = 488/663 nm) (Fig. S2d).

ROS generation and responsiveness of PP3–Se nanoparticles. The covalently linked porphyrin in the main chains of PP3–Se can generate ¹O₂ when irradiated with red light. Subsequently, we investigated the ROS production from the PP3–Se nanoparticles upon irradiation with a 660 nm laser. The Singlet Oxygen Sensor Green Reagent (SOSG, excitation/emission of reaction product 488 nm/

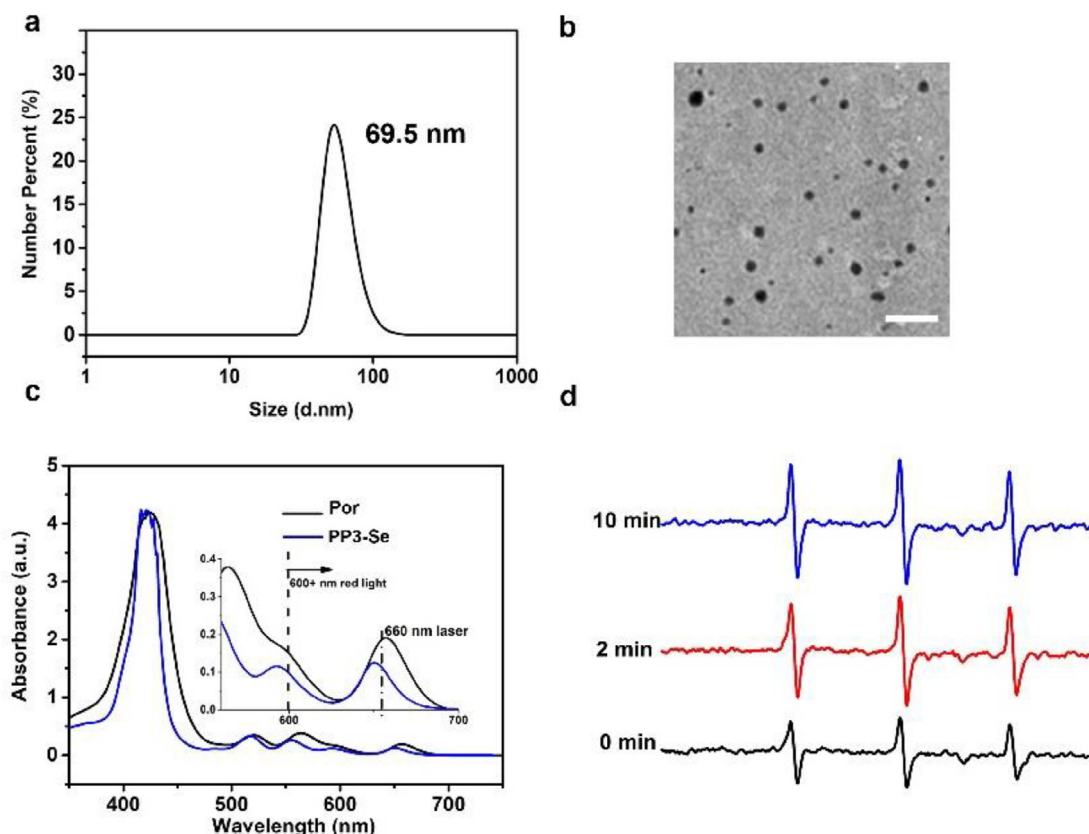


Fig. 1. Characterization of PP3-Se. a) Size distribution. b) TEM image (Scale bar = 1 μm). c) UV-Vis absorbance spectra of free Por and PP3-Se (concentration: PP3-Se = 0.5 mg/mL, Por = 0.1 mg/mL, solvent: DMF). d) ESR spectra of $^1\text{O}_2$ after laser irradiation to PP3-Se nanoparticles (1 mg/mL). 2,2,6,6-tetramethylpiperidine (30 mM) was used as a spin trap.

525 nm) was applied to determine the generation of $^1\text{O}_2$. Upon irradiation of PP3-Se for 4 min (660 nm, 1 W/cm²), a significant enhancement in the fluorescence intensity of the SOSG was detected at 525 nm (Fig. S2e). Meanwhile, the production of $^1\text{O}_2$ under irradiation could also be detected using electron spin-resonance spectroscopy (ESR) (Fig. 1d). Together, they confirmed the ROS generation of PP3-Se nanoparticles under red light irradiation.

According to previous work, selenium-inserted polymer aggregates could be oxidized by $^1\text{O}_2$ and further disassembled without main chain degradation [34]. However, in the selenoxide elimination reaction, carbon-selenium bonds could be oxidized and cleaved by ROS, leading to the production of acrylates (Fig. 2a). First, the response of PP3-Se nanoparticles was examined using the ^1H NMR spectrum and GPC. PP3-Se nanoparticles were irradiated with a 660 nm laser (1 W/cm²) at various exposure times (from 0 min to 6 min). The solutions were then freeze-dried to produce solids for following experiments. Part of the solids was dissolved into deuterium chloroform for ^1H NMR spectra measurements and the remaining parts were dissolved in DMF for the GPC test. Three new chemical shifts (between 5.5 and 6.7 ppm) belonging to acrylate was observed in the ^1H NMR spectra (Fig. 2b). When the PP3-Se nanoparticles were irradiated for 2 min, 30% of the β -seleno diesters would be oxidized and then eliminated to form acrylates. By prolonging the light exposure, the ratio of oxidation products slowly increased. GPC results were consistent with the ^1H NMR spectra (Fig. 2c). After irradiation, the peak corresponding to PP3-Se was widened, and its retention time was lengthened, indicating that the polymers were partially degraded. Meanwhile, some peaks associated with low molecular weight products appeared. For the PP6-Se polymer, only hydrogen belonging to α -C of selenoxide was found in the ^1H NMR spectra and no new peaks appeared in the GPC plots under the same treatment (Fig. S4e, S4f and S4g). X-ray photoelectron spectroscopy

(XPS) of Se^{3d} demonstrated that the binding energy of selenium in PP3-Se remained nearly unchanged, for selenide ether and elemental selenium share similar electronic configuration [35], while a new peak at 58.5 eV belonging to selenoxide appeared in PP6-Se after 2-min-irradiation (Fig. S4h).

To further verify the ROS responsiveness, the morphological transformation of PP3-Se nanoparticles with laser exposures was characterized by TEM. Unlike the barely changed self-assemble behavior of PP6-Se (Fig. S4i, Fig. S4j), the PP3-Se nanoparticles were first enlarged and then completely disassembled after longer exposure times (approximately 30 min) with a decrease in the mean count rate of nanoparticles (Fig. 2d, Fig. S3). These results, together with ^1H NMR spectra and GPC plots, indicated that photoinduced ROS could cleave the β -seleno diester linkers, leading to the degradation of PP3-Se nanoparticles and followed by the generation acrylates.

Endocytosis and anticancer activity of PP3-Se nanoparticles. Owing to the bioimaging capability of Por, PP3-Se nanoparticles could be used as a fluorescent probe to study endocytosis and intracellular distributions. MDA-MB-231 cells were incubated with PP3-Se nanoparticles and then examined at different time points by confocal laser scanning microscopy (CLSM) and flow cytometry (FCM). As shown in Fig. 3a, the cellular fluorescence intensity of PP3-Se was enhanced over time, which was consistent with the Por fluorescence signals measured by FCM (Fig. 3b), suggesting that the PP3-Se nanoparticles could be internalized continuously through intracellular endo/lysosomal transportation (Fig. S8a). Inductively coupled plasma mass spectrometry (ICP-MS) was also employed to measure the selenium concentration in blank, PP3-Se and PP6-Se treated group. These results further proved selenium-containing nanoparticles could be ingested by MDA-MB-231 cells (Fig. S9). Thus, the anticancer bioactivity of PP3-Se was further evaluated. MDA-MB-231, A549 and L-02 cell lines were co-

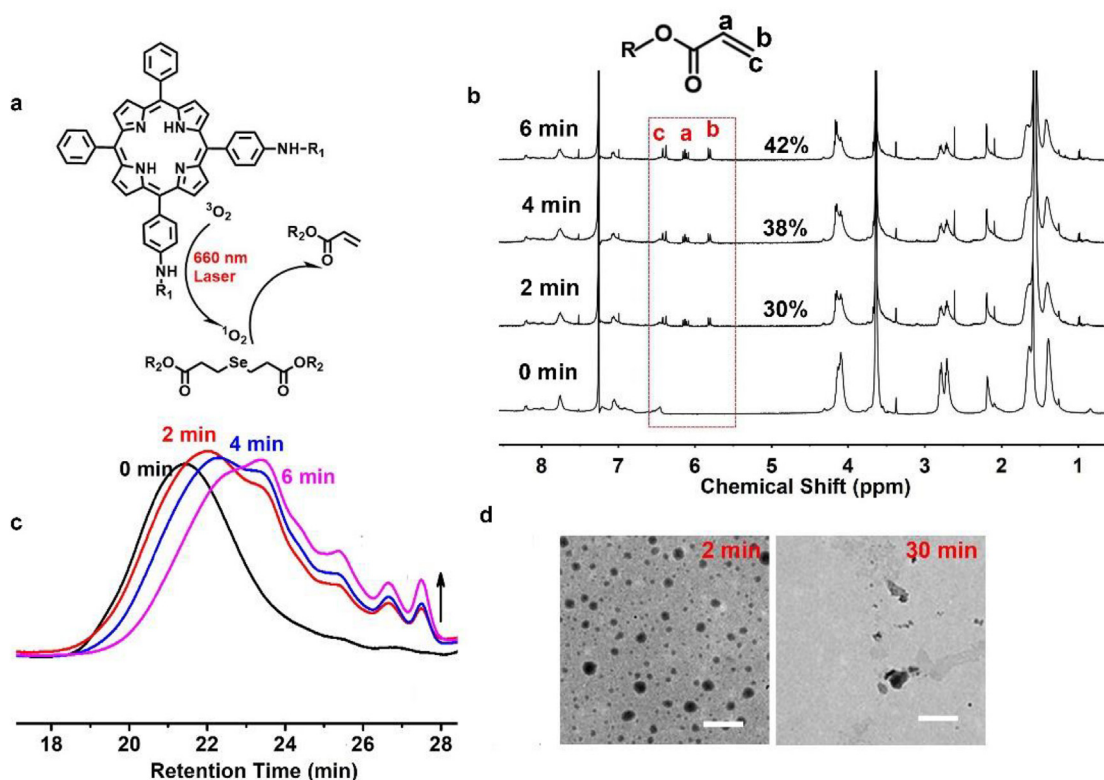


Fig. 2. Evidence of photoinduced selenoxide elimination. a) Mechanism of the oxidation of PP3-Se under light irradiation (660 nm, 1 W/cm^2). b) ^1H NMR spectra of PP3-Se after light irradiation (400 M, CDCl_3 , 25°C). c) GPC plots. d) TEM images of PP3-Se nanoparticles after light exposure (scale bar: $1 \mu\text{m}$).

incubated with PP3-Se nanoparticles at different concentrations without light irradiation. Cell viability was quantified using a CCK-8 assay. The results (Fig. S8b) demonstrated that PP3-Se nanoparticles exhibited almost no cytotoxicity to different cells without irradiation, even at a concentration of approximately $100 \mu\text{g/mL}$. The dark cytotoxicity of PP6-Se nanoparticles was also investigated in the same way with the MDA-MB-231 cell line and no cytotoxicity was observed (Fig. S8c).

The amounts of Por in PP3-Se and PP6-Se nanoparticle solutions were adjusted to the same concentration in the following cell experiments. All light illumination conditions were harmless to the above cell lines (Fig. S8d) and no obvious hyperthermia was observed in nanoparticle solutions under irradiation (Fig. S7b). After different exposure times to the laser (660 nm , 0.75 W/cm^2), significant cytotoxicity to MDA-MB-231 cells was found when co-incubated with PP3-Se nanoparticles for 72 h (Fig. 3c, Fig. S8e and Fig. S8f). Under the same irradiation time, the cytotoxicity of the PP3-Se nanoparticles group was distinctly higher than that of PP6-Se groups toward MDA-MB-231 cells (Fig. 3d). Even at a dosage of approximately 450 J/cm^2 , more than half of the cancer cells remained alive in the PP6-Se group after 72 h of co-incubation. In contrast, in the PP3-Se group, more than half of the cells were killed after a light dosage about 150 J/cm^2 . These results suggested that the photodynamic therapy of Por play a weak role in cytotoxicity. As such, we hypothesized that the elimination products, acrylates, may also possess antitumor capacities. To prove this assumption, H_2O_2 , one of the typical ROS in cancer cells, was employed. Poly-C6-C3(6)-Se nanoparticles were first oxidized by 1% H_2O_2 for 1 d. H_2O_2 was removed through dialysis. Then, the oxidation products were used in MDA-MB-231 and A549 cell cultures. As shown in Fig. S5c, after oxidation, the cytotoxicity of Poly-C6-C3-Se nanoparticles was significantly enhanced compared to Poly-C6-C6-Se both in the MDA-MB-231 and A549 cells. Similar results were also observed when MDA-MB-231 cells were co-cultured with PP3-Se nanoparticles and low concentrations of H_2O_2 (Fig. S6). 6-Hydroxyhexyl acrylate (HHA) was also

prepared as a model molecule of the PP3-Se oxidation products (Fig. S10). In MDA-MB-231 and A549 cells, the half-maximal inhibitory concentration (IC_{50}) values of HHA were approximately $400 \mu\text{M}$ and 3 mM , respectively (Fig. 3e). Both were lower than in L-O2 cells ($\text{IC}_{50} = 8 \text{ mM}$). These results might relate to the different expression levels of intracellular GSH or ROS [36]. These results were consistent with the PP3-Se nanoparticles under irradiation. From the above results, we could deduce that the ROS-triggered selenoxide elimination reaction could be induced by Por under irradiation. The elimination products could kill cancer cells and further improve antitumor efficiency.

Subsequently, the anticancer mechanism of PP3-Se nanoparticles under 660 nm irradiation was studied. As shown in Fig. 4a, after incubation for 48 h, there was no obvious apoptosis in the PP3-Se group (apoptotic ratio of 11.19%). A similar result was obtained for in the PP6-Se + L (L = light irradiation) group (a total apoptotic ratio of 8.18%) (Fig. S11a). However, in the PP3-Se + L group, the apoptotic ratio increased to 58.9%. When the irradiation time was reduced to 2 min, similar results were also found in PP3-Se and PP6-Se group (Fig. S11b). However, as shown in Fig. S13c, the HHA treatment significantly increased the early and late phases of cell apoptosis in a dose-dependent manner. These results implied that the elimination products, acrylates, improved the apoptosis-inducing ability. As shown in Fig. 4d, HHA could react with GSH under mild condition. And remarkable reduction in the reduced form of GSH levels was observed in MDA-MB-231 cells when treated with HHA or PP3-Se + L for 20 h (Fig. 4c). Meanwhile, total Glutathione or oxidized form of GSH were reduced or increased respectively in PP3-Se + L group (Fig. S12). 2,7-Dichlorodihydrofluorescein diacetate (DCFH-DA) was employed as a probe to indicate the generation of ROS. After incubation with or without PP3-Se nanoparticles for 24 h, the fluorescence intensities in MDA-MB-231 cells stained by DCFH-DA were observed. In the PP3-Se group, the ROS level increased slightly (2.80%–6.85% for the control group) which might be related to the acrylates produced by the microenvironment of the

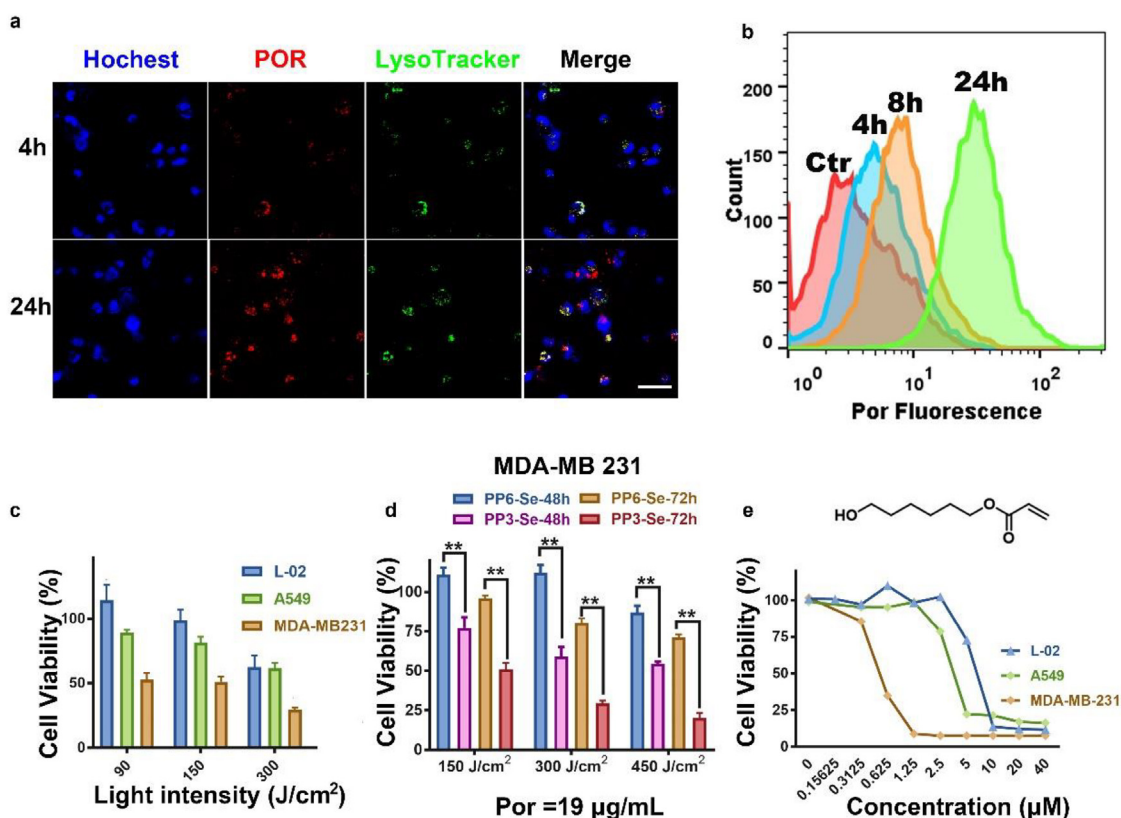


Fig. 3. Cellular uptake and cytotoxicity of PP3-Se nanoparticles. a) cellular uptake of PP3-Se nanoparticles. CLSM images of MDA-MB-231 cells stained with LysoTracker Green and Hoechst 33342 after 4 or 24 h incubation with PP3-Se nanoparticles at the dose of 100 µg/mL (Por concentration = 19 µg/mL). b) FCM analysis of the Por fluorescence intensity in MDA-MB-231 cells. c) Cytotoxicity of PP3-Se under irradiation (660 nm, 0.75 W/cm², n = 3). d) Normalized viability of MDA-MB-231 cells treated with PP3-Se and PP6-Se nanoparticles after 48 or 72 h incubation under 4–10 min irradiation. The results were repeated three times, independently. Error bars denote mean ± s.d., **p < 0.01. Statistical significance was assessed by Student t-test (paired, two tailed). e) Cytotoxicity of HHA toward MDA-MB-231, A549 and L-02 cells after 72 h incubation. (For interpretation of the references to colour in this figure legend, the reader is referred to the Web version of this article.)

cancer cells. Under light irradiation, Por could transfer energy from light to intracellular ³O₂ to generate ROS, and then greatly increase intracellular ROS levels (59.7%) (Fig. 4e). In addition, after 20 h of light irradiation, an increase in DCF fluorescence intensity in the presence of oxidized and eliminated PP3-Se nanoparticles (from 2.40% to 14.9%) indicated that acrylates, generated by the oxidation of intracellular ROS and ¹O₂, might increase intracellular oxidative stress. These results were further proved by HHA. (Fig. S13d). Glutathione peroxidase (GPx) and catalase (CAT) could convert H₂O₂ to water, while superoxide anion in cytosol could be converted to H₂O₂ by superoxide dismutase (SOD). As shown in Fig. S14, the activity of SOD and the expression GPx was downregulated in PP3-Se + L group, while the expression of CAT was upregulated. Highly increased H₂O₂ would inhibit the enzymatic activity of SOD, while a decrease in GSH levels caused downregulation of the expression of GPx. Consequently, increased H₂O₂ formation increased the activity of CAT. However, glutathione S-transferase (GST) was upregulated in PP3-Se + L group which might catalyze the reaction between acrylate and glutathione (Fig. S14c). We deduced that the elimination products, acrylates, could act as antioxidant inhibitor and induce cell apoptosis through the depletion of GSH levels and the generation of oxidative stress.

Increased ROS formation induced by acrylates could cause DNA damage, which might lead to cell cycle arrest and could markedly regulate the level of apoptosis-related protein [37]. During DNA replication, S-phase checkpoints can be activated once cells encounter damage to their DNA, slowing the progression of S phase [38]. S phase arrest was found in the PP3-Se + L group (Fig. 4b). After 24 h of cell culture, the number of cells in S phase increased slightly from 40.35%

in the untreated group to 47.16% in the PP3-Se + L group. Whereas in PP3-Se group, the number of S phase cells was similar to the untreated group. As shown in Fig. S13e, HHA caused a concentration-related delay of the cell cycle in S phase. Cyclin-dependent kinase inhibitor 1A (P21) plays an important role in cell cycle arrest, so the expression of P21 was also measured. As shown in Figs. S15a and 20 h after light irradiation, P21 was upregulated in MDA-MB-231 cells in PP3-Se + L group. ROS-damaged mitochondrial tend to release cytochrome c (Cytc) into cytosol, and further activate the mitochondrial-mediated apoptosis. We therefore measured the expression of Cytc in MDA-MB-231. In PP3-Se + L group, the Cytc expression was upregulated (Fig. S15 b). Bcl-2 protein family acts as the key regulator in intrinsic mitochondrial apoptosis. Among them, Bax and Bcl-2 are two-well known proteins related to proapoptotic and anti-apoptotic effects [39,40]. As shown in Fig. 4g, Western blot analysis revealed that 10 min to 20 h after light irradiation, the expression of Bcl-2 decreased significantly while the expression of Bax gradually increased in the PP3-Se + L group. Meanwhile, in the PP6-Se + L group, even 20 h after light irradiation, there were no obvious changes in the expressions of Bax and Bcl-2. These results were consistent with the HHA treatment cells (Fig. S13b). Compared to the untreated and light group, caspase 3 and caspase 8 in the MDA-MB-231 cells were all upregulated to different degrees in the PP3-Se + L group or HHA groups, which implied that death receptor mediated apoptotic pathway was also activated (Fig. 4f and Fig. S13a). These results further proved that acrylate, generated through the ROS-triggered selenoxide elimination reaction, was the key cause of cell apoptosis to MDA-MB-231 cancer cells.

In vivo drug delivery and antitumor treatment. Nanomedicines

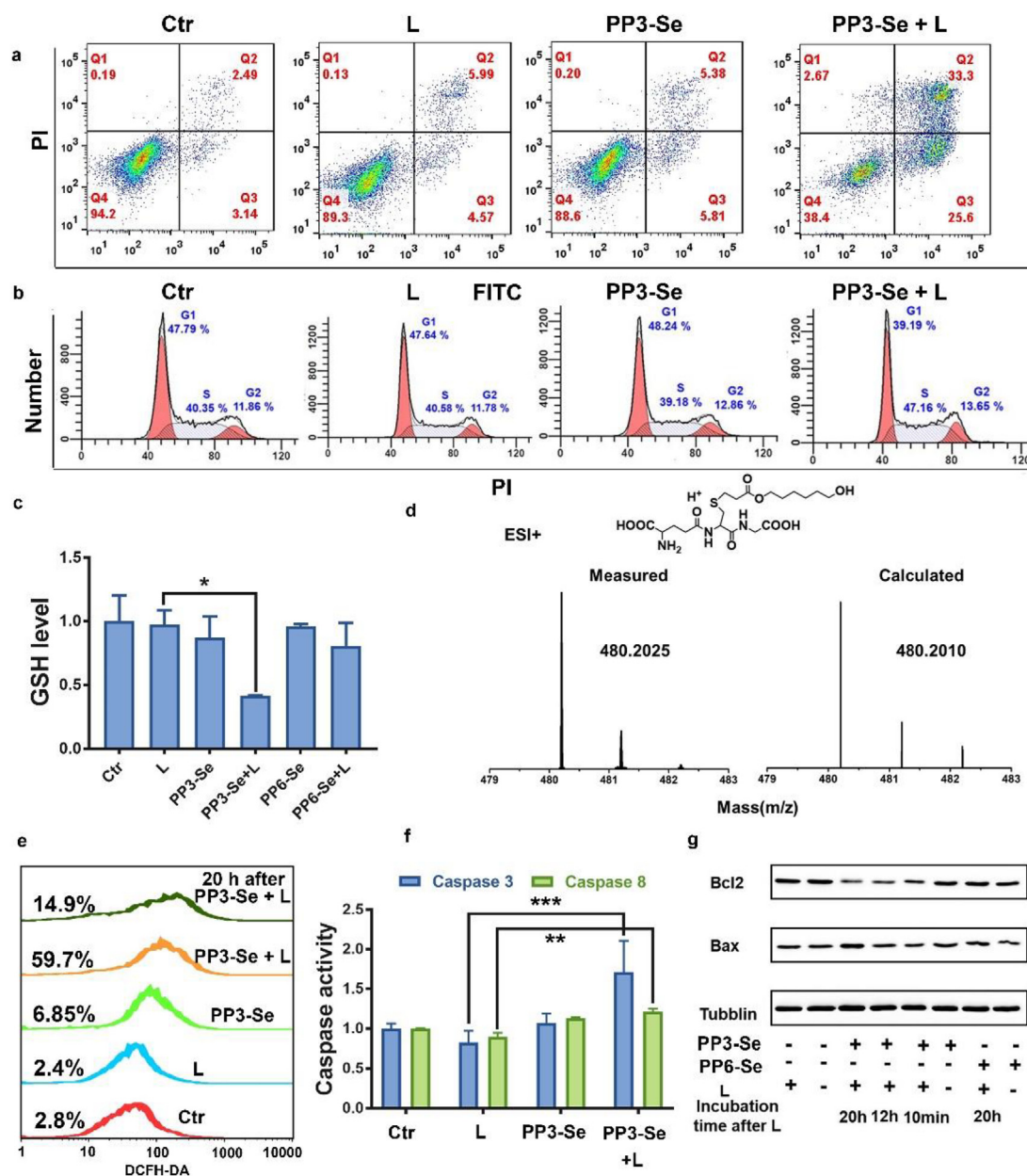


Fig. 4. Mechanism of PP3-Se nanoparticles induced apoptosis, concentration of PP3-Se nanoparticles 100 $\mu\text{g}/\text{mL}$ and PP6-Se = 174 $\mu\text{g}/\text{mL}$ in all experiments. **a)** FCM analysis of MDA-MB-231 cell apoptosis induced by PP3-Se nanoparticles with or without light (660 nm laser, 0.75 W/cm², 4 min). **b)** Distribution of cells in G1, S and G2 phase after a 24 h exposure to PP3-Se nanoparticles with or without light. **c)** Depletion of GSH by various treatment of PP3-Se (100 $\mu\text{g}/\text{mL}$) and PP6-Se (174 $\mu\text{g}/\text{mL}$) nanoparticles in MDA-MB-231 cells using DNTB (5,5'-dithiobis (2-nitrobenzoic acid) kit. **d)** Equal mole GSH and HHA (10 mM) were dissolved into mixed solvent (DMF: water = 1:10) and then reacted at 37 °C for 3 h. The mixture was then measured by electrospray ionization (ESI), peak belonging to their chemical combination product was observed. **e)** ROS detected through FCM analysis. **f)** Influences of PP3-Se nanoparticles with or without light on caspase 3 and caspase 8 activity levels. The results were repeated three times, independently. Error bars denote mean \pm s.d., ** p < 0.01, *** p < 0.001. Statistical significance was assessed by Student t-test (paired, two tailed). **g)** Western blot analysis of the expression of Bcl2 and Bax protein.

with suitable diameters can be accumulated in tumors through enhanced permeability and retention (EPR) effects [41,42]. To investigate whether PP3-Se nanoparticles could have the EPR effect *in vivo*, MDA-MB-231 cell-bearing nude mice were intravenously injected with saline or PP3-Se nanoparticles. As shown in Fig. S16a, PP3-Se nanoparticles exhibited a time-dependent tumor accumulation, which implied that PP3-Se nanoparticles could survive from being adsorbed by protein or cleared by the reticuloendothelial system during the long circulation in mice. We then monitored the concentration of selenium in tumors at different timepoints by ICP-MS. Our results were consistent with the *ex vivo* fluorescence imaging. Even at 24 h after administration, the accumulation of PP3-Se nanoparticles was maintained in tumors due to

the PEG modification (Fig. S16b). These results demonstrated that PP3-Se nanoparticles exhibited an excellent delivery to tumor cells *in vivo*.

To evaluate the *in vivo* therapeutic efficacy of the 660 nm laser-mediated therapy nanoplatform, MDA-MB-231 orthotopically xenografted tumor-bearing nude mice were chosen and divided into 7 groups. When the tumors reached a predetermined size (approximately 100 mm³), we began the tail-intravenous injections with different formulations, including saline, PP3-Se nanoparticles and PP6-Se nanoparticles. The laser treatment was performed for a total of 4 or 10 min at a power density of 0.75 W/cm² with a 1 min interval after every 2 min of exposure. As shown in Fig. 5a and Fig. 5c, the tumors treated with

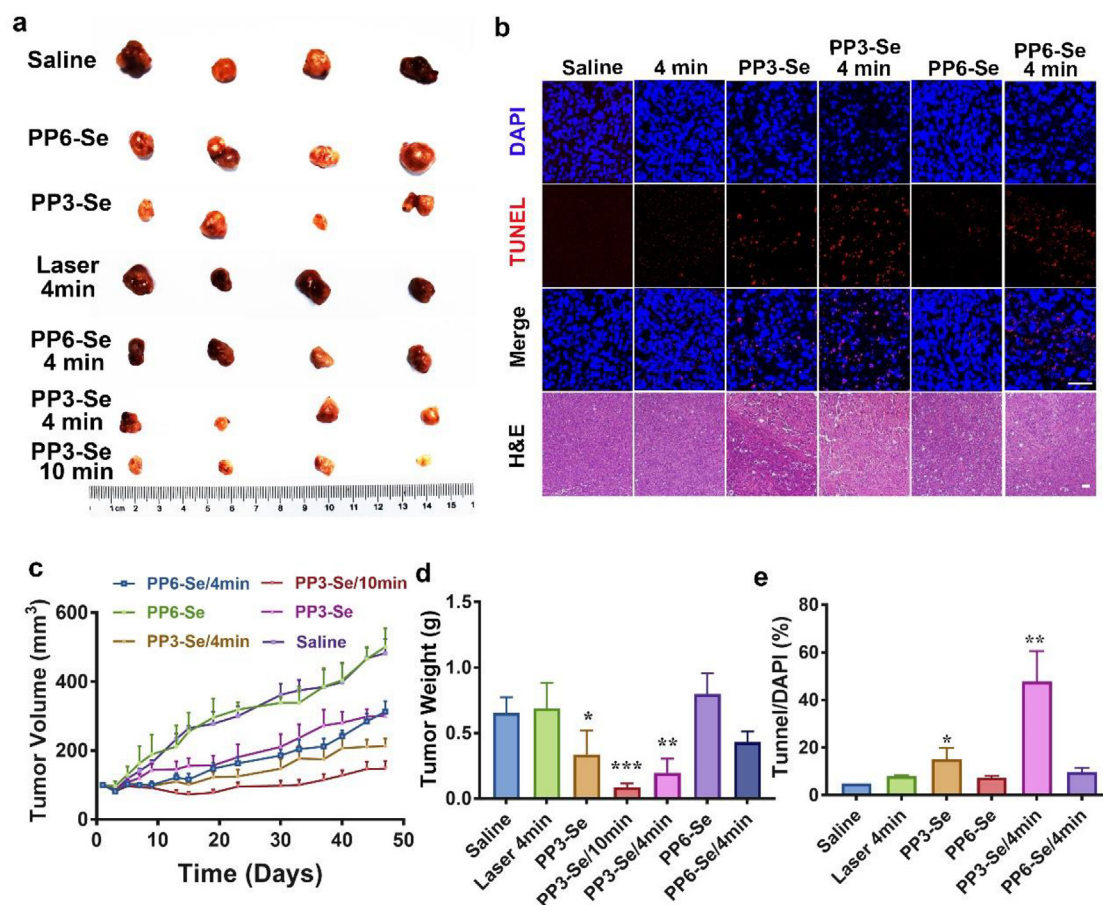


Fig. 5. Antitumor effects in orthotopically xenografts MDA-MB-231 tumor-bearing nude mice. **a)** Tumor volume images of various drug formulations. **b)** Representative TUNEL (scale bar: 50 μ m) and H&E (scale bar: 200 μ m) sections of the tumors. **c)** Tumor growth curves. **d)** Tumor weight in various treatment groups. **e)** Apoptosis degrees after treatment with different drug formulations. The results in **d** and **e** were repeated seven and three times, independently. Error bars denote mean \pm s.d., * p < 0.05, ** p < 0.01, *** p < 0.001, compared to Saline group. Statistical significance was assessed by Student t-test (paired, two tailed).

saline and blank PP6-Se nanoparticles (19.3 mg/kg, 2.1 mg Por/kg) grew progressively. However, for the mice treated with blank PP3-Se nanoparticles (11.1 mg/kg, 2.1 mg Por/kg), a certain delay of the tumor growth was observed, which was similar with the PDT therapy efficiency of PP6-Se/4 min. A similar phenomenon was also observed in cell experiments. As shown in Fig. S17, when co-cultured with 500 μ g/mL PP3-Se for 48 h, half of the MDA-MB-231 cells were killed, whereas at the same Por concentration, PP6-Se was almost nontoxic. These results indicated that PP3-Se nanoparticles would first accumulate in tumor tissue, after which the selenoxide elimination reaction could be triggered by the high ROS levels in cancer cells to produce acrylates and inhibit tumor growth. While in the PP3-Se/4 min and PP3-Se/10 min group, a more effective repression of cancer progression was observed due to the generation of more acrylates after laser irradiation. These results were consistent with the growth curves and tumor images (Fig. 5d). To validate the extent of apoptosis in the tumors after various treatments, H&E and TUNEL staining were performed (Fig. 5b and e). Only basal level apoptosis could be found in saline, 4 min light, and PP6-Se groups. While in PP3-Se, PP6-Se/4 min and PP3-Se/4 min groups, apoptosis with different degrees was observed. These results demonstrated that PP3-Se could be oxidized by ROS, further enhancing the antitumor effects under laser exposure.

Subsequently, we focused on the side effects of PP3-Se with or without light in mice. Five groups were studied: saline control, PP3-Se, PP3-Se/4 min, PP6-Se, PP6-Se/4 min. Mice slowly gained weight in all groups, as shown in Fig. S18a. In addition, no obvious changes in organ morphology for the heart, liver, spleen, lungs and kidneys, based on H&E staining (Fig. S18b). Blood chemistry/haematology detection of

serum further confirmed the safety of PP3-Se with or without light (Fig. S18c, Fig. S18d and Fig. S19). Hence, we deduced that low doses of acrylates generated by endo/exogenous ROS through oxidation and elimination were almost harmless to the body.

4. Conclusion

In summary, the selenoxide elimination reaction was, for the first time, introduced into nanomedicine mediated cancer therapy. β -seleno diesters containing nanoparticle could be oxidized and further eliminated by intracellular ROS to produce acrylates with antitumor capabilities. With photosensitizers introduced into this system, the elimination process could be accelerated by $^1\text{O}_2$ generated under light irradiation. The elimination product, acrylates, increased ROS levels and apoptosis in tumor cells, and finally improved anticancer activity in the mice tumor model. This selenoxide elimination reaction has extensive application prospect in the field of biodegradable nanomedicine. Moreover, different from traditional ROS-responsive linkers, β -seleno diesters could regenerate cytotoxic ROS and further disturb the redox balance of the tumor cells more effectively and specifically. In addition, the combination between this structural design with photosensitizers would achieve a persistent generation of ROS for sustainable phototherapy even under dark conditions. We anticipate this ROS-manipulation method will provide more opportunities for efficient cancer treatment.

Acknowledgements

This work was financially supported by the National Basic Research Plan of China (2018YFA0208900), the National Natural Science Foundation of China (21734006), National Science Foundation for Distinguished Young Scholars (21425416), the Foundation for Innovative Research Groups of the National Natural Science Foundation of China (21821001).

We thank Core Facility of Center of Biomedical Analysis, Tsinghua University for assistance with cell imaging and Flow cytometry analysis. And we thank professor Dongsheng Liu's group for the Confocal Microscopy.

Appendix A. Supplementary data

Supplementary data to this article can be found online at <https://doi.org/10.1016/j.biomaterials.2019.119514>.

Author contributions

C.S. designed and performed the experiments. C.S. and L.W. synthesized the monomer. C.S. S.G., B.X. and T.L. performed the mechanistic study, S.G. and H.X. conceived and supervised the project. C.S., S.G. and H.X. wrote the manuscript. All authors discussed the results.

Competing financial interests

The authors declare no competing financial interests.

References

- A. Glasauer, N.S. Chandel, Targeting antioxidants for cancer therapy, *Biochem. Pharmacol.* 92 (2014) 90–101.
- F. Li, T. Li, X. Han, H. Zhuang, G. Nie, H. Xu, Nanomedicine assembled by co-ordinated selenium-platinum complexes can selectively induce cytotoxicity in cancer cells by targeting the glutathione Antioxidant defense system, *ACS Biomater. Sci. Eng.* 4 (2018) 1954–1962.
- B.C. Dickinson, C.J. Chang, Chemistry and biology of reactive oxygen species in signaling or stress responses, *Nat. Chem. Biol.* 7 (2011) 504–511.
- M. Giorgio, M. Trinei, E. Migliaccio, P.G. Pelicci, Hydrogen peroxide: a metabolic by-product or a common mediator of ageing signals? *Nat. Rev. Mol. Cell Biol.* 8 (2007) 722–728.
- Z.T. Schafer, A.R. Grassian, L. Song, Z. Jiang, Z. Gerhart-Hines, H.Y. Irie, S. Gao, P. Puigserver, J.S. Brugge, Antioxidant and oncogene rescue of metabolic defects caused by loss of matrix attachment, *Nature* 461 (2009) 109–115.
- J. Noh, B. Kwon, E. Han, M. Park, W. Yang, W. Cho, W. Yoo, G. Khang, D. Lee, Amplification of oxidative stress by a dual stimuli-responsive hybrid drug enhances cancer cell death, *Nat. Commun.* 6 (2015) 6907–6916.
- B. Yang, Y. Chen, J. Shi, Reactive oxygen species (ROS)-based Nanomedicine, *Chem. Rev.* 119 (2019) 4881–4985.
- D. Dolmans, D. Fukumura, R.K. Jain, Photodynamic therapy for cancer, *Nat. Rev. Cancer* 3 (2003) 380–387.
- Y. Li, T.Y. Lin, Y. Luo, Q. Liu, W. Xiao, W. Guo, D. Lac, H. Zhang, C. Feng, S. Wachsmann-hogiu, J.H. Walton, S.R. Cherry, D., J. Rowland, D. Kukis, C. Pan, S.K. Lam, A smart and versatile theranostic nanomedicine platform based on nanoporphyrin, *Nat. Commun.* 5 (2014) 4712–4727.
- K. Yamagishi, I. Kirino, I. Takahashi, H. Amano, S. Takeoka, Y. Morimoto, T. Fujie, Tissue-adhesive wirelessly powered optoelectronic device for metronomic photodynamic cancer therapy, *Nat. Biomed. Eng.* 3 (2019) 27–36.
- B. Ma, S. Wang, F. Liu, S. Zhang, J. Duan, Z. Li, Y. Kong, Y. Sang, H. Liu, W. Bu, L. Li, Self-assembled copper-amino acid nanoparticles for in situ glutathione “and” H₂O₂ sequentially triggered chemodynamic therapy, *J. Am. Chem. Soc.* 141 (2019) 849–857.
- J. Fan, M. Peng, H. Wang, H. Zheng, Z. Liu, C. Li, X. Wang, X. Liu, S. Cheng, X. Zhang, Engineered bacterial bioreactor for tumor therapy via Fenton-like reaction with localized H₂O₂ generation, *Adv. Mater.* (2019) 1808278.
- Bai, J., Jia, X., Zhen, W., Cheng, W., Jiang, X. A facile ion-doping strategy to regulate tumor microenvironments for enhanced multimodal tumor theranostics. *J. Am. Chem. Soc.* 140(180), 106–109.
- H. Xu, W. Cao, X. Zhang, Selenium-containing polymers: promising biomaterials for controlled release and enzyme mimics, *Acc. Chem. Res.* 46 (2013) 1647–1658.
- W. Cao, L. Wang, H. Xu, Selenium/tellurium containing polymer materials in nanobiotechnology, *Nano Today* 10 (2015) 717–736.
- N. Ma, Y. Li, H. Xu, Z. Wang, X. Zhang, Dual redox responsive assemblies formed from diselenide block copolymers, *J. Am. Chem. Soc.* 132 (2010) 442–443.
- W. Cao, X. Zhang, X. Miao, Z. Yang, H. Xu, γ -Ray-responsive supramolecular hydrogel based on a diselenide-containing polymer and a peptide, *Angew. Chem. Int. Ed.* 52 (2013) 6233–6237.
- X. Hu, G. Liu, Y. Li, X. Wang, S. Liu, Cell-penetrating hyperbranched polyprodrug amphiphiles for synergistic reductive milieu-triggered drug release and enhanced magnetic resonance signals, *J. Am. Chem. Soc.* 137 (2015) 362–368.
- X.Q. Li, H.Y. Wen, H.Q. Dong, W.M. Xue, G.M. Pauletti, X.J. Cai, W.J. Xia, D. Shi, Y.Y. Li, Self-assembling nanomicelles of a novel camptothecin prodrug engineered with a redox-responsive release mechanism, *Chem. Commun.* 47 (2011) 8647–8649.
- P. Pei, C. Sun, W. Tao, J. Li, X. Yang, J. Wang, ROS-sensitive thioether-linked polyphosphoester-doxorubicin conjugate for precise phototriggered locoregional chemotherapy, *Biomaterials* 188 (2019) 74–82.
- A. Napoli, M. Valentini, N. Tirelli, M. Müller, J.A. Hubbell, Oxidation-responsive polymeric vesicles, *Nat. Mater.* 3 (2004) 183–189.
- M. Wang, S. Sun, C.I. Neufeld, B. Perez-Ramirez, Q. Xu, Reactive oxygen species-responsive protein modification and its intracellular delivery for targeted cancer therapy, *Angew. Chem. Int. Ed.* 53 (2014) 13444–13448.
- J. Shi, P.W. Kantoff, R. Wooster, O.C. Farokhzad, *Nat. Rev. Cancer* 17 (2017) 20–37.
- W.H. Tao, Z.G. He, ROS-responsive drug delivery system for biomedical applications, *Asian J. Pharm. Sci.* 13 (2018) 101–112.
- E. Cabane, X. Zhang, K. Longowska, G.G. Palivan, W. Meier, Stimuli-responsive polymers and their applications in nanomedicine, *Biointerphases* 7 (2012) 1–27.
- J. Fang, T. Seki, H. Maeda, Therapeutic strategies by modulating oxygen stress in cancer and inflammation, *Adv. Drug Deliv. Rev.* 61 (2019) 290–302.
- G. Huang, H. Chen, Y. Dong, X. Luo, H. Yu, Z. Moore, E.A. Bey, D.A. Boothman, J. Gao, Superparamagnetic iron oxide nanoparticles: amplifying ROS stress to improve anticancer drug efficacy, *Theranostics* 3 (2013) 116–126.
- H. Schweikl, C. Petzel, C. Bolay, K. Hiller, W. Buchalla, S. Krifka, 2-hydroxyethyl methacrylate-induced apoptosis through the ATM- and p53-dependent intrinsic mitochondrial pathway, *Biomaterials* 35 (2014) 2890–2904.
- S. Krifka, K. Hiller, G. Spagnuolo, A. Jewett, G. Schmalz, H. Schweikl, The influence of glutathione on redox regulation by antioxidant proteins and apoptosis in macrophages exposed to 2-hydroxyethyl methacrylate (HEMA), *Biomaterials* 33 (2012) 5177–5186.
- L. Wang, K. Zhu, W. Cao, C. Sun, C. Lu, H. Xu, ROS-triggered degradation of selenide-containing polymers based on selenoxide elimination, *Polym. Chem.* 10 (2019) 2039–2046.
- K.B. Sharpless, R.F. Lauer, A.Y. Teranishi, Electrophilic and nucleophilic organoselenium reagents. New routes to α,β -unsaturated carbonyl compounds, *J. Am. Chem. Soc.* 95 (1973) 6137–6139.
- M. Yang, T. Yang, C. Mao, Enhancement of photodynamic cancer therapy by physical and chemical factors, *Angew. Chem. Int. Ed.* (2019), <https://doi.org/10.1002/anie.201814098> Accepted Article.
- C. Sun, S. Ji, F. Li, H. Xu, Diselenide-containing hyperbranched polymer with light-induced cytotoxicity, *ACS Appl. Mater. Interfaces* 9 (2017) 12924–12929.
- Y. Wang, Y. Deng, H. Luo, A. Zhu, H. Ke, H. Yang, H. Chen, Light-responsive nanoparticles for highly efficient cytoplasmic delivery of anticancer agents, *ACS Nano* 11 (2017) 12134–12144.
- J.F. Moulder, W.F. Stickle, P.E. Sobol, K.D. Bomben, Handbook of x-ray photoelectron spectra, Appendix B. Chemical State Tables, Physical Electronics Division 55344 Perkin-Elmer, Eden Prairie, MN, 1992, pp. 91–93.
- E. Olm, K. Jonsson-Videsater, I. Ribera-Cortada, A.P. Fernandes, L.C. Eriksson, S. Lehmann, A. Rundlof, C. Paul, Selenite is a potent cytotoxic agent for human primary AML cells, *Cancer Lett.* 282 (2009) 116–123.
- D. Moon, M. Kim, Y.H. Choi, J.W. Hyun, W.Y. Chang, G. Kin, Butein induces G₂/M phase arrest and apoptosis in human hepatoma cancer cells through ROS generation, *Cancer Lett.* 288 (2010) 204–213.
- E.M. Noonan, D. Shah, M.B. Yaffe, D.A. Lauffenburger, L.D. Samson, O⁶-Methylguanine DNA lesions induce an intra-S-phase arrest from which cells exit into apoptosis governed by early and late multi-pathway signalling network activation, *Integr. Biol.* 4 (2012) 1237–1255.
- Z.N. Oltvai, C.L. Milliman, S.J. Korsmeyer, Bcl-2 heterodimerizes *in vivo* with a conserved homolog, Bax, that accelerates programmed cell death, *Cell* 74 (1993) 609–619.
- E. Yang, J. Zha, J. Jockel, L.H. Boise, C.B. Thompson, S.J. Korsmeyer, Bad, a heterodimeric partner for Bcl-XL and Bcl-2, displaces Bax and promotes cell death, *Cell* 80 (1995) 285–291.
- G. Yu, M. Zhang, M.L. Saha, Z. Mao, J. Chen, Y. Yao, Z. Zhou, Y. Liu, C. Gao, F. Huang, X. Chen, P.S. Stang, Antitumor activity of a unique polymer that incorporates a fluorescent self-assembled metallacycle, *J. Am. Chem. Soc.* 139 (2017) 15940–15949.
- K. Knop, R. Hoogenboom, D. Fischer, U.S. Schubert, Poly(ethylene glycol) in drug delivery: pros and cons as well as potential alternatives, *Angew. Chem. Int. Ed.* 49 (2010) 6288–6308.